ECAS 2022

MDPI

Proceeding Paper

Moisture Transport and Contribution to the Continental Precipitation †

Yazhu Yang [1,2], Niansen Ou [1,2,*], Chunlei Liu [1,2,*], Xiaoqing Liao [1,2], Ning Cao [1,2] and Rayimaay Yusup [3]

[1] South China Sea Institute of Marine Meteorology, Guangdong Ocean University, Zhanjiang, China; email (Y.Y.); email (X.L.); email (N.C.)
[2] CMA-GDOU Joint Laboratory for Marine Meteorology, Guangdong Ocean University, Zhanjiang, China
[3] Meteorological Office of Xinjiang, China; email
* Correspondence: nsou@gdou.edu.cn (N.O.); liuclei@gdou.edu.cn (C,L.)
† Presented at 5th International Electronic Conference on Atmospheric Sciences, 16–31 July 2022; Available online: https://ecas2022.sciforum.net/.

Abstract: Understanding the water cycle change under the warming climate is essential, particularly the ocean to land moisture transport, which affects the precipitation over land areas. Using ERA5 data from 1988–2020, the moisture transport and its trend around the boundary of each continent, including the Eurasia, Africa, North America, South America, Antarctic, Australia and Greenland, have been investigated. The inflow and outflow sections of the moisture have been identified for each continent. The trends of moisture convergence over Eurasia, Africa, North America, Antarctic and Australia have positive trends, with the value of 1.78 ± 3.11, 2.43 ± 3.16, 12.92 ± 2.27 and 0.34 ± 0.45 (in 10^6 kg/s/decade), respectively, but only the trend over North America is statistically significant at 0.1 significance level. The moisture convergence trend of −0.87 ± 3.64 (in 10^6 kg/s/decade) over South America is negative but insignificant. The positive trend of 0.04 ± 0.35 (in 10^6 kg/s/decade) over Greenland is very weak. Both evaporation and moisture convergence (or transport) contribute to the continental precipitation, but the convergence dominates the precipitation variability over all continents, and the correlation coefficients between the time series of continental mean convergence and precipitation anomalies are higher than 0.8 in all continents.

Keywords: moisture transport; convergence; precipitation; trend

Academic Editor: *Anthony Lupo*

Published: 14 July 2022

1. Introduction

Precipitation is a part of the water cycle and it is essential for the society. Precipitation is closely related to the moisture transport, particularly over land areas where the moisture is transported from oceans to land. How will the precipitation change under the warming climate? It is an important question to answer.

Many research results have shown that "wet getting wetter and dry getting drier" [1–4], and the corresponding atmospheric circulation is getting slower [1]. This circulation change will definitely affect the moisture transport from ocean to land, therefore affecting the precipitation.

In this study, we will use the ERA5 atmospheric reanalysis data over 1988–2020 to investigate the large scale moisture transport from ocean to continents, in order to have a clear idea how these transports have changed under the warming climate. The inflow and outflow of the vertically integrated total column moisture from different boundary sections will be described and the area convergence trend will be presented.

2. Data and Methods

The precipitation, evaporation, vertically integrated eastward and northward moisture fluxes and the moisture convergence from ERA5 atmospheric reanalysis will be used

in this study. Although there is a mass conservation problem in the reanalysis data, the effect on the moisture transport is small [5], therefore the results are reliable. The selected period is from 1988–2020 (33 years), in order to make comparison with observations in the future study.

There are seven continents and they are Eurasia, Africa, North America, South America, Antarctica, Australia and Greenland. The time series trend is tested by the two-sided Wald Test with t-distribution at significant level of 90%.

3. Moisture Transport to the Continents

In order to study the moisture transport through the continent boundaries, the integrated fluxes along the boundary and their trend are investigated for seven continental areas. The moisture transport through the boundaries of each continent is plotted in Figure 1. The left column of Figure 1 is the multiannual mean (1988–2020) showing the moisture flux magnitude and transport direction (arrow), the color along the boundary indicates the flux density in kg m^{-1} s^{-1}. The warm color means the inflow of the moisture to the area and the cold color means the outflow of the moisture. The boundary is divided into several sections mainly based on the boundary orientation and marked by the solid black circles. The moisture transport is integrated by distance anticlockwisely from the starting point of section A along the boundary as shown in the second column, together with the color representing the slope (in kg m^{-1} s^{-1}) of the curve. The positive slope means the inflow of the moisture to the region and the negative slope means the outflow, which share the same meaning and scale as the first column. Some rising sections are marked and their seasonal climatology and interannual time series are plotted in the last two columns.

For the Eurasia continent, the average moisture inflows along sections A, B and C are 212.8 × 10^6, 68.13 × 10^6, 208.57 × 10^6 kg s^{-1}, and the moisture outflows of sections D and E are −149.3 × 10^6 and -33.4 × 10^6 kg s^{-1}, respectively. The net moisture transport to the Eurasia continent is 306.79 × 10^6 kg s^{-1}. The intense moisture inflow is mainly from the Atlantic for section A, and it is mainly from the west coast of the Mediterranean Sea and the Red Sea for section B. The most intense inflow in section C is from Somali jet traveling through Arabian Sea and reaching the west coast of India, contributing to the Indian monsoon [6] and east Asia monsoon, and the integrated moisture inflow along this section is about 208.57 × 10^6 kg s^{-1}. However after precipitating over India, the rest moisture flows out from the east coast and crosses the Bay of Bengal to reach the south coast of Asia. The moisture inflow along the Bay of Bengal contributes the most and the quantity is about 200 × 10^6 kg s^{-1}. It is also noticed there are two intense inflow sections in boundary D, one is along the coast of South China Sea, and another one along the west coast of Korean Peninsula. The integrated inflows are 75.05 × 10^6 and 79.77 × 10^6 kg s^{-1}, respectively.

Along the Africa continent boundary, the average moisture inflow is 227.11 × 10^6 in section B and 14.17 × 10^6 kg s^{-1} in section C. It is worth noting that the water vapor inflow in C has a significant increase trend（5.58 × 10^6 kg/s/decade）, and the moisture outflow along section A is −142.42 × 10^6 kg s^{-1} . The net moisture transport to the Africa continent is about 99.48 × 10^6 kg s^{-1}.

The general feature of the the moisture flow is the inflow from the east coast and the outflow from the west coast of Africa, and the contribution from the north boundary is small (Figure 1d2). Southeast coast is very distinct and the major moisture sources are from the tropical and subtropical Western Indian Ocean (0–30° S) mainly in the summer. The dense moisture inflow from the east coast is partly associated with the cutoff lows [8] and the tropical storms/cyclones around Mozambique, Madagascar and Mauritius [7].The outstanding feature is the continued accumulation of moisture from the east coast and the amount is about 300 × 10^6 kg s^{-1}. It is related to both the ARs (Atomspheric River) and LLJs (low-level jets). Another increasing part of section A is also related to the AR. The precipitation seasonal variability in Africa is dominated by the ITCZ (Intertropical Convergence Zone) movement and monsoons. The tropical precipitation associated with the ITCZ is not as strong as those over other longitudes partly due to its long traveling path of ITCZ

[9]. But the ITCZ has complicated location and changes, which needs to be further investigated. The mean flow in Figure 1c2 cannot reflect the west African monsoon well, since the moisture inflow from the south boundary of the west Africa is mainly from the southwesterly of the west African monsoon, which cannot be seen from the mean flow. The seasonal variability of the flux in section A22 shows the onset and finish months. The area mean Africa precipitation is bimodal, consistent with the main moisture inflow from sections A21 and B21.

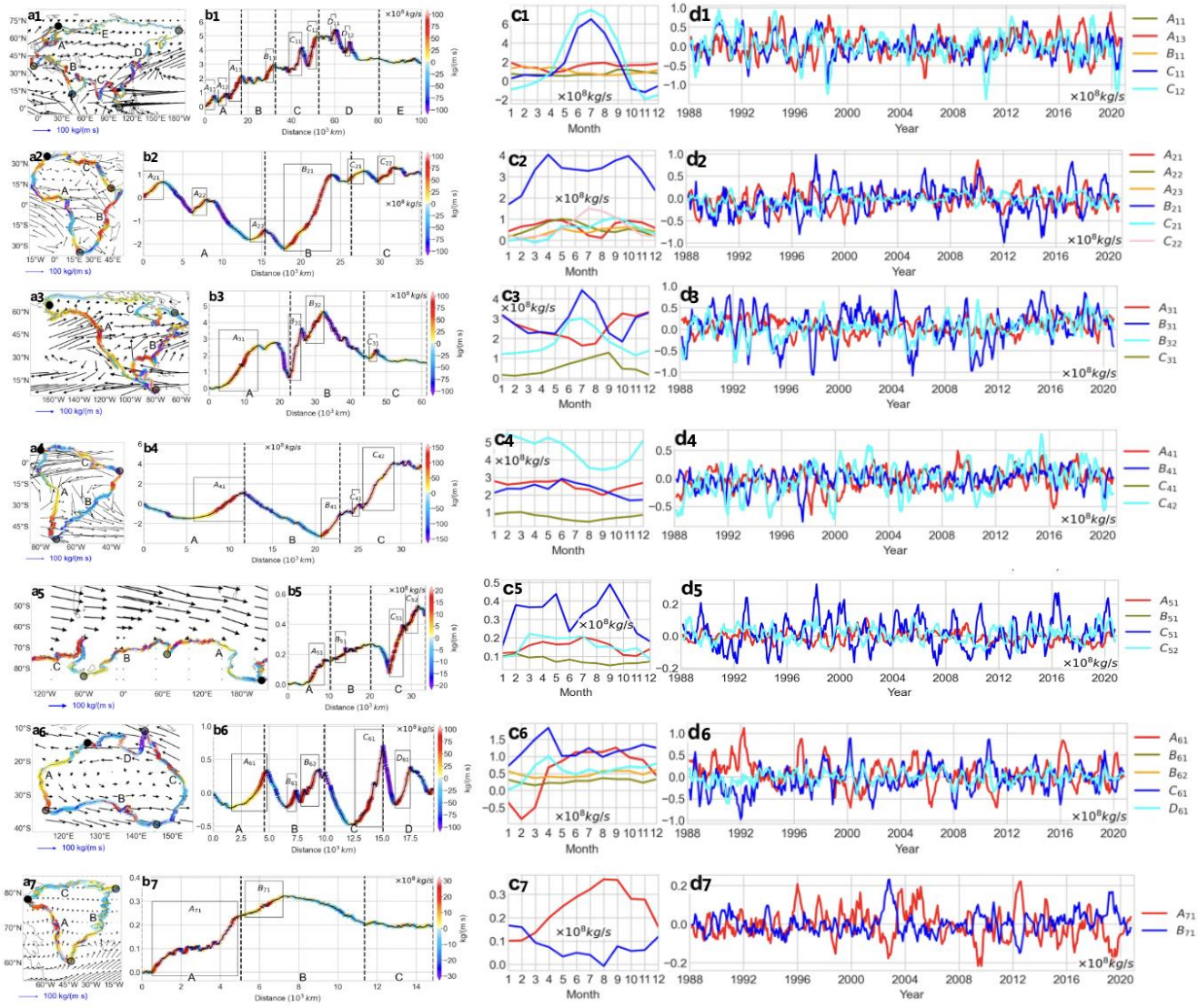

Figure 1. Left column shows the seven continents and arrows are climatological moisture flux vectors. Colors along the boundary indicate inflow (warm color) and outflow (cold color) of the moisture. The boundary of each continent is divided into different sections. The second column is the accumulation of the moisture flux integrated anticlockwisely from section A. The colors share the same meaning and scale as the first column. Some strong inflow sections are marked (such as A_{11}, A_{13}). The third column shows the climatology of moisture inflow for marked sections in the second column. The last column shows the anomaly time series of the inflow over marked sections in the second column.

Over North America continent, the average moisture inflow is 73.7 × 10^6 kg s^{-1} along west coast and 120.15 × 10^6 kg s^{-1} along east coast, and the moisture outflow along north coast is -36.06 × 10^6 kg s^{-1}. The net moisture inflow to the North America is 157.79 × 10^6 kg s^{-1}, and the increase trend of 12.92 × 10^6 kg/s/decade is statistically significant.

For Australian continent, the easterly crosses the northern area, so there is a rapid increase of the moisture inflow from sections C61 and D61. Their seasonal variations show the monsoon characteristics from November to April. The flux variability and the area mean precipitation over the land area has significant correlation coefficient of 0.50, implying that the fluxes through C61 and D61 are the main source of the precipitation there [10,11]. Another main moisture inflow is from the west coast and it is about 70×10^6 kg s^{-1}.

Due to the page limit, results for other areas are not discussed here and some characteristics can be found in Tables 1 and 2. The trends of Q_{net} are 1.78 ± 3.11 (Eurasia), 2.43 ± 3.16 (Africa), 12.92 ± 2.27 (North Ameica), −0.87 ± 3.64 (South America), 0.34 ± 0.45 (Antarctic), 3.48 ± 2.45 (Australia) and 0.04 ± 0.35 (Greenland) (in unit of 10^6 kg/s/decade).

Table 1. Multi-annual mean (units: 10^6 kg/s) and trend of moisture flux (units: 10^6 kg/s/decade) through the sections in Figure 1.

Eurasia	QA	QB	QC	QD	QE	Qnet
annual mean	212.8	68.13	208.57	-149.3	-33.4	306.79
trend	3.21 ± 3.42	−4.65 ± 2.44	1.18 ± 4.48	3.13 ± 4.84	−1.09 ± 1.99	1.78 ± 3.11
Africa	QA	QB	QC	Qnet		
annual mean	-142.42	227.11	14.78	99.48		
trend	8.59 ± 4.38	5.43 ± 3.62	5.58 ± 2.66 *	2.43 ± 3.16		
North America	QA	QB	QC	Qnet		
annual mean	73.7	120.15	-36.06	157.79		
trend	7.75 ± 4.08	4.11 ± 3.62	1.06 ± 1.52	12.92 ± 2.27 *		
South America	QA	QB	QC	Qnet		
annual mean	113.46	-215.87	485.21	382.8		
trend	−7.03 ± 3.19 *	1.77 ± 3.32	4.39 ± 3.05	−0.87 ± 3.64		
Antarctic	QA	QB	QC	Qnet		
annual mean	15.33	11.13	19.35	45.81		
trend	−0.41 ± 0.28	0.71 ± 0.24 *	0.05 ± 0.37	0.34 ± 0.45		
Australia	QA	QB	QC	QD	Qnet	
annual mean	29.85	-0.9	40.57	-65.94	3.57	
trend	−7.83 ± 3.06 *	3.39 ± 2.52	8.87 ± 4.21 *	−0.95 ± 2.91	3.48 ± 2.45	
Greenland	QA	QB	QC	Qnet		
annual mean	23.98	-3.64	-1.2	19.14		
trend	−1.24 ± 0.83	1.90 ± 0.82 *	−0.62 ± 0.39	0.04 ± 0.35		

* indicate statistically significant by two-sided Wald Test with t-distribution at $\alpha = 0.1$ significance level.

Table 2. Multi-annual mean (units: 10^6 kg/s) and trend of moisture flux (units: 10^6 kg/s/decade) through the sections in Figure 1.

Eurasia	A_{11}	A_{12}	A_{13}	B_{11}	C_{11}	C_{12}	D_{11}	D_{12}
annual mean	77.34	60.98	156.17	104.29	173.49	209.71	75.05	79.77
trend	0.87 ± 2.59	1.82 ± 2.37	3.44 ± 3.46	1.30 ± 1.51	−2.95 ± 3.40	−5.39 ± 3.95	−2.14 ± 2.31	1.15 ± 1.85
Africa	A_{21}	A_{22}	A_{23}	B_{21}	C_{21}	C_{22}		
annual mean	65.78	54.27	40.78	315.83	47.08	61.31		
trend	1.47 ± 2.19	−0.98 ± 0.64	1.17 ± 0.99	5.44 ± 3.33	4.36 ± 1.24 *	0.32 ± 1.28		
North America	A_{31}	B_{31}	B_{32}	C_{31}				
annual mean	256.31	287.97	178.15	53.44				
trend	2.59 ± 1.96	1.64 ± 3.78	7.79 ± 2.60 *	−1.80 ± 1.53				
South America	A_{41}	B_{41}	C_{41}	C_{42}				
annual mean	255.41	229.83	76	459.69				
trend	3.98 ± 1.96 *	4.16 ± 2.05 *	1.88 ± 0.51 *	9.93 ± 2.59 *				
Antarctic	A_{51}	B_{51}	C_{51}	C_{52}				
annual mean	15.08	7.77	32.48	15.82				
trend	−0.77 ± 0.38 *	0.43 ± 0.22 *	0.70 ± 1.00	−0.20 ± 0.52				
Australia	A_{61}	B_{61}	B_{62}	C_{61}	D_{61}			
annual mean	56.52	27.24	48.19	119.22	57.79			
trend	−5.69 ± 2.83 *	1.32 ± 0.72 *	1.77 ± 1.11*	8.07 ± 3.42	1.62 ± 1.97			
Greenland	A_{71}	B_{71}						
annual mean	23.72	7.74						
trend	−0.96 ± 0.81	1.02 ± 0.62						

* indicate statistically significant by two-sided Wald Test with t-distribution at $\alpha = 0.1$ significance level.

4. Moisture Contribution to the Continental Precipitation

The left column of Figure 2 shows the seasonal changes of precipitation, evaporation and VIMC (Vertically Integrated Moisture Convergence) for each continent from 1988 to 2020. The right column shows the anomaly time series of these three variables. It can be seen that the evaporation contributes more in quantity to precipitation than VIMC over the land at middle and low latitudes. However, the anomaly time series of precipitation and VIMC are significantly positively correlated, and their correlation coefficients are 0.82 (Eurasia), 0.80 (Africa), 0.85 (North Ameica), 0.90 (South America), 0.99 (Antarctic), 0.85 (Australia) and 0.97 (Greenland), respectively, implying the dominance of the moisture transport in the precipitation variability.

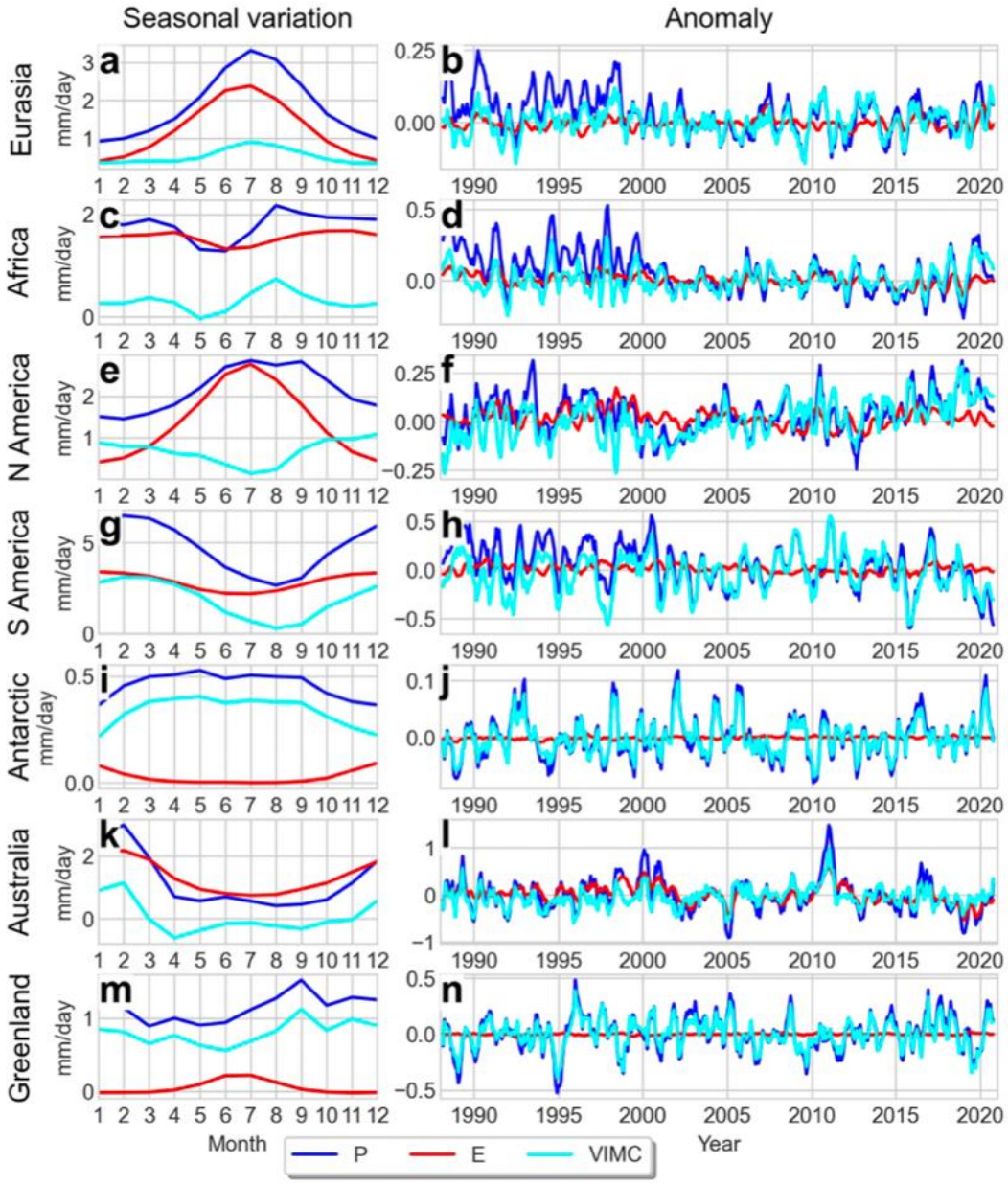

Figure 2. Left column is the seasonal changes of precipitation, evaporation and VIMC (Vertically Integrated Moisture Convergence) for each continent averaged over 1988 to 2020. The right column is the anomaly time series of these three variables.

5. Discussion and Conclusions

In this study, the moisture convergences over seven continents are studied. Although all trends are positive except for the South America where the moisture convergence showed a weak decreasing trend, only the moisture transport to the North America shows statistically significant increase. The inflow and outflow of the moisture along the continent boundary are also investigated in details and the sections with intense inflow have been identified and listed in Table 2. Over the middle and low latitude continents, the evaporation is the main contributor in quatity to the continental precipitation, but the moisture convergence dominates the variability of the precipitation.

The relationship between the intense inflow and outflow is not well investigated and will be further investigated in the future study.

Author Contributions:

Funding:

Institutional Review Board Statement:

Informed Consent Statement:

Data Availability Statement: The ERA5 reanalysis data are downloaded at https://cds.climate.copernicus.eu/cdsapp#!/search?type=dataset.

Acknowledgments: This work is supported by the National Natural Science Foundation of China (42075036), Fujian Key Laboratory of Severe Weather (2021KFKT02), and the scientific research start-up grant of Guangdong Ocean University (R20001). Xiaoqing Liao and Yazhu Yang are also supported by the Postgraduate Education Innovation Project of Guangdong Ocean University (202144, 202253).

Conflicts of Interest: The authors declare no conflict of interest.

References

1. Held, I.M.; Soden, B.J. Robust Responses of the Hydrological Cycle to Global Warming. *J. Clim.* **2006**, *19*, 5686–5699. https://doi.org/10.1175/JCLI3990.1.
2. Liu, C.; Allan, R.P.; Huffman, G.J. Co-Variation of Temperature and Precipitation in CMIP5 Models and Satellite Observations. *Geophys. Res. Lett.* **2012**, *39*. https://doi.org/10.1029/2012GL052093.
3. Liu, C.; Allan, R.P. Multisatellite Observed Responses of Precipitation and Its Extremes to Interannual Climate Variability. *J. Geophys. Res. Atmos.* **2012**, *117*. https://doi.org/10.1029/2011JD016568.
4. Allan, R.P.; Liu, C.; Loeb, N.G.; Palmer, M.D.; Roberts, M.; Smith, D.; Vidale, P.L. Changes in Global Net Radiative Imbalance 1985–2012. *Geophys. Res. Lett.* **2014**, *41*, 5588–5597. https://doi.org/10.1002/2014GL060962.
5. Mayer, J.; Mayer, M.; Haimberger, L. Consistency and Homogeneity of Atmospheric Energy, Moisture, and Mass Budgets in ERA5. *J. Clim.* **2021**, 1–69. https://doi.org/10.1175/JCLI-D-20-0676.1.
6. Boos, W.R.; Emanuel, K.A. Annual Intensification of the Somali Jet in a Quasi-Equilibrium Framework: Observational Composites. *Q. J. R. Meteorol. Soc.* **2009**, *135*, 319–335. https://doi.org/10.1002/qj.388.
7. Klinman, M.G.; Reason, C.J.C. On the Peculiar Storm Track of TC Favio during the 2006–2007 Southwest Indian Ocean Tropical Cyclone Season and Relationships to ENSO. *Meteorol. Atmos. Phys.* **2008**, *100*, 233–242. https://doi.org/10.1007/s00703-008-0306-7.
8. Singleton, A.T.; Reason, C. Variability in the Characteristics of Cut-off Low Pressure Systems over Subtropical Southern Africa. *Int. J. Climatol.* **2010**, *27*, 295–310. https://doi.org/10.1002/JOC.1399.
9. Liu, C.; Liao, X.; Qiu, J.; Yang, Y.; Feng, X.; Allan, R.P.; Cao, N.; Long, J.; Xu, J. Observed Variability of Intertropical Convergence Zone over 1998–2018. *Environ. Res. Lett.* **2020**, *15*, 104011. https://doi.org/10.1088/1748-9326/aba033.
10. Pope, M.; Jakob, C.; Reeder, M.J. Regimes of the North Australian Wet Season. *J. Clim.* **2010**, *22*, 6699–6715. https://doi.org/10.1175/2009JCLI3057.1.
11. Ren, L.; Arkin, P.; Smith, T.M.; Shen, S. Global Precipitation Trends in 1900–2005 from a Reconstruction and Coupled Model Simulations. *J. Geophys. Res. Atmos.* **2013**, *118*, 1679–1689. https://doi.org/10.1002/jgrd.50212.